

Contact-Induced Semiconductor-to-Metal Transition in Single-Layer WS_2

Maciej Dendzik, Albert Bruix, Matteo Michiardi, Arlette S. Ngankeu, Marco Bianchi, Jill A. Miwa, Bjørk Hammer, Philip Hofmann, and Charlotte E. Sanders*

Department of Physics and Astronomy, Interdisciplinary Nanoscience Center, Aarhus University, 8000 Aarhus C, Denmark

E-mail: sanders.charlotte@phys.au.dk

Phone: +45 871 55585. Fax: +45 861 20740

Abstract

Low-resistance ohmic contacts are a challenge for electronic devices based on two-dimensional materials. We show that an atomically precise junction between a two-dimensional semiconductor and a metallic contact can lead to a semiconductor-to-metal transition in the two-dimensional material—a finding which points the way to a possible method of achieving low-resistance junctions. Specifically, single-layer WS_2 undergoes a semiconductor-to-metal transition when epitaxially grown on $\text{Ag}(111)$, while it remains a direct band gap semiconductor on $\text{Au}(111)$. The metallicity of the single layer on $\text{Ag}(111)$ is established by lineshape analysis of core level photoemission spectra. Angle-resolved photoemission spectroscopy locates the metallic states near the Q point of the WS_2 Brillouin zone. Density functional theory calculations show that the metallic states arise from hybridization between Ag bulk bands and the local conduction band minimum of WS_2 near the Q point.

Introduction

Low-resistance metal-semiconductor contacts are an essential ingredient of electronic devices. This subject is well understood for bulk materials,¹ but is one of the biggest hurdles for the exploitation of novel single-layer (SL) semiconductors such as MoS₂ or WS₂.² The contact resistance between a metal and a semiconductor is, in general, influenced by several factors, such as the heights of the Schottky and tunnel barriers and the degree of hybridization between the materials. These parameters cannot be inferred from the equilibrium properties of the materials in a simple way, particularly in the case of SL materials. The Schottky barrier, for instance, which depends on the SL semiconductor’s electronic structure, can be affected by a gap renormalization in the presence of an underlying metal.³

One way to achieve a low-resistance junction and avoid the occurrence of a tunneling barrier is to induce a local semiconductor-to-metal transition in the SL material itself—for example, via a local structural phase transition from the semiconducting trigonal prismatic (“1H”) polymorph to the metallic 1T polymorph of a transition metal dichalcogenide.^{4–8} However, from the standpoint of device applications, the practical utility of this approach has so far been limited by the difficulty of controllably patterning 1H/1T device structures within the SL, and also by the instability of the 1T phase.

Recent theoretical work has suggested an alternative approach: a semiconductor-to-metal transition induced simply by interaction of the SL with its substrate.^{2,9–11} This is difficult to realize in practice because it requires a perfect interface between the substrate and the SL.^{12,13} Here we show that a semiconductor-to-metal transition can indeed occur in a SL semiconductor having an atomically well-defined interface with an appropriately chosen substrate. We find that SL WS₂ remains semiconducting on Au(111) but undergoes a semiconductor-to-metal transition on Ag(111). This transition results from the combination of the Ag(111) surface’s lower work function and a hybridization between the conduction bands of WS₂ and Ag; together, these lead to the emergence of metallic bands with strong WS₂ character at the Q point of the WS₂ Brillouin zone. We directly observe the metalliza-

tion of the SL via the asymmetry of the lineshape of the W 4f core level (CL) photoemission spectrum.

The implications are significant, not only in that the creation of ohmic contacts is an important requirement for device applications: The present results dovetail with recent findings that the substrate can control the size of the band gap in SL materials^{14,15} as well as the strength and character of doping.^{16,17} Combining these effects, one could create complex two-dimensional electronic circuits, in which metallic wires are contacted to semiconducting devices with controllable p or n doping and tunable band gaps, all in a single SL semiconductor prepared on a suitably pre-patterned substrate material.

Methods

Sample Preparation and Characterization

The epitaxial growth method used here is similar to that which has been described previously for related material systems.¹⁸⁻²⁰ Substrates were prepared by Ne⁺ sputtering and annealing in ultra-high vacuum. W was evaporated onto the clean substrate surfaces at room temperature in an H₂S atmosphere, and samples were subsequently annealed to approximately 825~925 K while being continually exposed to H₂S. Scanning tunneling microscopy (STM) confirmed coverage of ca. 0.7 monolayers (similar results were also seen for higher coverage up to 1.1 monolayers). STM and low-energy electron diffraction (LEED) showed that the hexagonal atomic structure, the moiré superstructure, and the domain size of WS₂/Ag(111) were similar to those of WS₂/Au(111), which has been characterized elsewhere in detail.^{18,21}

All experiments were performed at the SGM3 beamline of the ASTRID2 synchrotron radiation source.²² Sample growth and measurement were carried out *in situ*, without breaking vacuum. STM measurements were made at room temperature. The sample temperature of angle-resolved photoemission spectroscopy (ARPES) and LEED measurements was approximately 100 K. The energy and angular resolution of the ARPES measurements were better

than 30 meV and 0.2° , respectively. X-ray photoemission spectroscopy (XPS) from shallow CLs indicated that the WS_2 on Ag(111) sample had negligible Se contamination of around 2% of a monolayer.

Theoretical Methods

The electronic structure calculations were carried out using the periodic density functional theory code VASP.²³⁻²⁵ The valence electrons were described with plane-wave basis sets with a kinetic energy threshold of 415 eV, and the interaction between the valence and frozen core-electrons was accounted for by means of the projector-augmented-wave method of Blöchl.²⁶ The PBE approximation to the exchange-correlation functional was used²⁷ in combination with the DFT-D3 method of Grimme correction to account for vdW interactions.

The supercell models consist of a $\sqrt{13} \times \sqrt{13}$ R13.9° cell of WS_2 on a 6-layer 4×4 cell of the metal (111) surface. This model is smaller than the experimentally identified moiré lattice, but it allows solving the inherent mismatch between WS_2 and metal lattices while applying a minimal strain on the metal ($<0.2\%$). The geometry of the supercells was optimized until the forces on all atoms were smaller than $0.01 \text{ eV}\text{\AA}^{-1}$. All atoms were relaxed except those in the 4 lowermost metal layers, which were kept in their truncated bulk positions. A $(4 \times 4 \times 1)$ mesh of k -points was used to sample the reciprocal space during geometry optimizations, and the charge density was subsequently recalculated with a single point calculation using a denser $(10 \times 10 \times 1)$ mesh of k -points. An energy threshold of 10^{-6} eV was used to define convergence of the self-consistent field of the electron density.

For the supercell models, the band structure along the high symmetry directions of the primitive cell of WS_2 is folded into the smaller reciprocal lattice of the supercell. In order to recover the unfolded band structure with the symmetry of the primitive unit cell of WS_2 , we have calculated the effective band structure using the method proposed by Popescu and Zunger²⁸ as implemented in the BandUp code.^{29,30} Spin-orbit coupling has been included for all band structure calculations using the virtual crystal approximation as implemented

in the VASP code.³¹

Results and Discussion

STM and LEED measurements show close structural similarity between WS₂ grown on Au(111) and on Ag(111), including the morié pattern formed between SL and substrate, as seen in the insets of Fig. 1 and in Refs.^{18,21,32} However, XPS reveals that the two systems have entirely different electronic characters: This manifests itself in the shape of the W 4f CL spectra. To understand this difference, one must first notice that in Fig. 1 the spectra obtained from samples grown on each of the two types of substrates (Au and Ag) consist of the 7/2-5/2 doublet, each peak of which is itself fittable by two components, one of higher intensity and one of lower intensity. The higher-intensity component arises from the WS₂ basal plane, and the lower-intensity component from edge atoms or partially-sulphided WS_{2-x} clusters.^{33,34}

The key difference between the spectra from samples prepared on each of the two substrates is the lineshapes of the high-intensity peaks. For WS₂/Au(111), these can be fitted by Gaussian-broadened Lorentzians, as expected for CLs of semiconducting materials, and as has also been observed for WS₂ on transition metal oxides.³⁵ By contrast, the peak shapes for WS₂/Ag(111) cannot be decomposed into a small number of Lorentzians, because of their asymmetric lineshape consisting of a tail at high binding energy. This is particularly clear in Fig. 1(c), which shows the high-intensity components of the two systems superimposed and shifted so that the peak maxima coincide. The asymmetric lineshape is fit best by a Doniach-Šunjić profile, a profile in which a Gaussian-broadened Lorentzian is modified by an asymmetry parameter that describes low-energy electron-hole interactions during the photoemission process.^{36,37} While many factors can influence the shape of the CL peak, the particular asymmetry embodied by the Doniach-Šunjić lineshape is a definite signature of metallicity. (The reverse is not necessarily true: not all metals exhibit an asymmetrical peak

shape.) Fitting of the CLs of WS₂/Ag(111) (described in detail in the supplementary materials) gives an asymmetry parameter of 0.10(1) for the high-intensity components, consistent with the asymmetry of other, typical metallic systems.^{21,38} Thus, although WS₂/Au(111) may retain its semiconducting character, WS₂/Ag(111) is metallic. We note that neither a presence of the metallic 1T phase nor edge states can be responsible for the asymmetric line shape observed here, since both have characteristic CL peaks at *lower* binding energies.^{34,39–41} Moreover, there are no signatures of the 1T phase’s distinctively different band structure in the ARPES data, and significant contributions from edge states seem unlikely since the STM data reveals the formation of large islands.

An additional experimental observation relating to the metallicity of WS₂/Ag(111) lies in the absolute binding energy of the 4f CLs: Specifically, the CL WS₂/Ag(111) peaks are shifted toward higher binding energy than those of WS₂/Au(111) by approximately 207(20) meV, whereas the corresponding shift of the valence band states is significantly larger (275(24) meV—see below). As already mentioned, the different work functions of Ag(111) and Au(111) lead to different Fermi level pinning in the two systems, explaining a shift of the valence band. However, the different shift in the CL binding energies relative to the valence states in the two systems suggests a mechanism beyond a purely electrostatic shift. A plausible explanation for this difference is local final state screening that affects the core level binding energies. In a metallic system, the core hole can be screened by the electrons at the Fermi level, leading to higher kinetic energy of the escaping photoelectron. These screening effects depend crucially on the local electronic structure around the emitting atom.^{34,43} The observation of a decreased binding energy / increased kinetic energy for the core electrons from WS₂/Ag(111) is thus consistent with a metallic SL.

The metallic character of WS₂/Ag(111) should be identifiable in the electronic band structure as measured by ARPES. Fig. 2(a) and (b) show the photoemission intensity resulting from such a measurement along the Γ - K direction of the Brillouin zone for WS₂ grown on (a) Ag(111) and (b) Au(111). In both cases, the upper valence band (VB) of

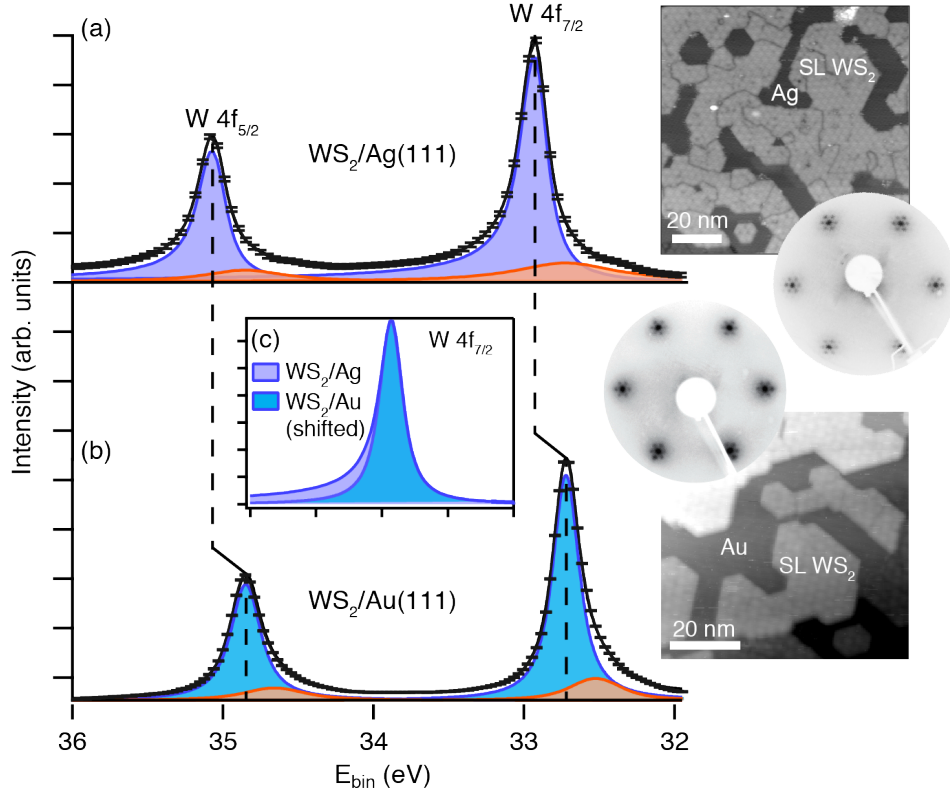


Figure 1: Direct evidence of metallic SL WS₂ on Ag(111) from CL spectroscopy. (a)–(b) CL spectra (acquired at photon energy $h\nu=140$ eV) from the W 4f states of (a) WS₂/Ag(111) and (b) WS₂/Au(111). Data points are black crosses; the black line is the fit; blue and orange peaks correspond to WS₂ and incompletely sulphided WS_{2-x} clusters, respectively.³⁴ (c) Comparison of the fitted W 4f_{7/2} components for WS₂/Ag(111) and WS₂/Au(111), shifted and normalized so that the peak maxima coincide. The insets show STM images and LEED patterns of WS₂ grown on Ag(111) and Au(111), respectively.⁴² STM imaging parameters are 0.09 nA and 1.43 V in (a) and 0.58 nA and 1.16 V in (b). The electron kinetic energy for LEED is 114 eV.

WS₂ with the spin-split VB maximum at K is clearly identified and the dispersion is very similar to that calculated for a free-standing SL, shifted such that the VB maximum coincides with the measurement (blue dashed line).^{18,21} A distortion of the bands near Γ is consistent with previous observations of SL MoS₂/Au(111) and SL WS₂/Au(111),^{18,19,44} and will be discussed below. The VB maximum in WS₂/Ag(111) is at a higher binding energy than in WS₂/Au(111) (by ca. 0.28 eV).

The metallic behaviour of WS₂/Ag(111) has to be caused by additional states near the Fermi energy and these should give rise to ARPES features that cannot be attributed to the substrate. Indeed, as can be seen in Fig. 2(a), (c) and (e), there is a diffuse feature at the Fermi level along Γ - K , marked by white arrows. These states are absent for clean Ag scanned at the same photon energy.²¹ Faint states can also be seen in this location in the data set acquired from WS₂/Au(111), but they are extremely weak in that case. We can therefore conclude that similar physical mechanisms are at work in both systems, and that the difference in the density of states (DOS) at the Fermi level between the two systems is a quantitative effect rather than a qualitative one. However, the effect is so weak in the case of WS₂/Au(111) that the system essentially retains its semiconducting character and shows no detectable sign of metallicity in CL spectroscopy (Fig. 2(b), (d) and (f)).

We now discuss several possible scenarios to explain these findings. The obvious interpretation is that of a band crossing from a state just above the Fermi level, such that a shallow electron pocket is formed. The simplest scenario to achieve this would be a rigid shift of the conduction band (CB) to lower energies. The calculated lowest CB for free-standing SL WS₂ is superimposed on the data in Fig. 2(a), aligning the dispersion such that the CB minimum at K is found at the same energy as recently reported from a time-resolved pump/probe ARPES experiment for the same system.³² Assuming that the two material systems (WS₂/Ag(111) and WS₂/Au(111)) exhibit a similar size of the renormalized band gap, the CB is expected to be closer to the Fermi energy for WS₂/Ag(111) than for WS₂/Au(111) because of the different work function of the two metal surfaces, leading to the observed

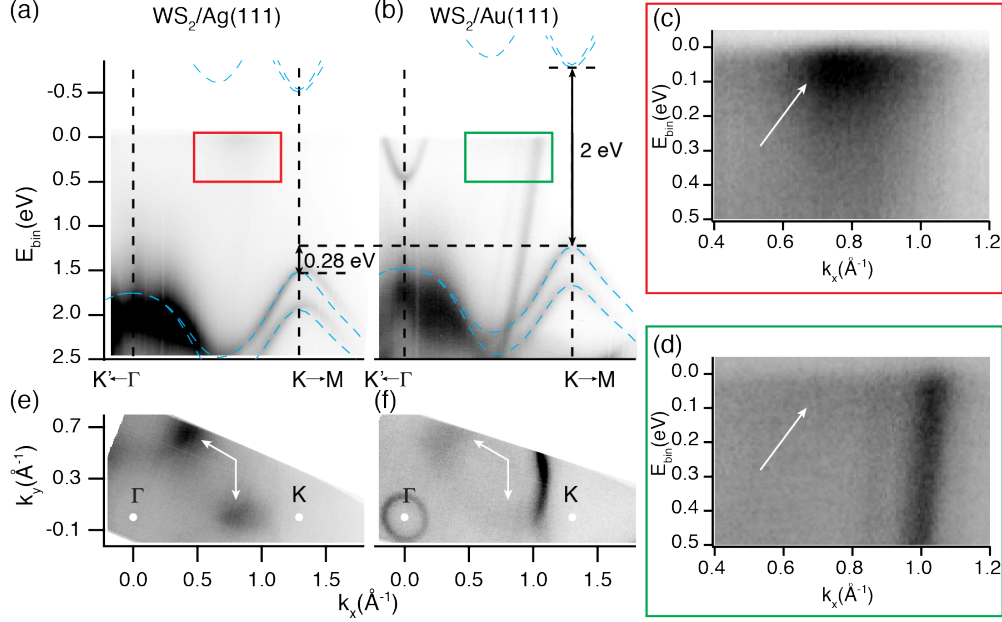


Figure 2: Electronic structure of SL WS_2 on $\text{Ag}(111)$ and $\text{Au}(111)$ from ARPES, with evidence for metallic states in the former system. (a)–(b) Photoemission intensity along the high-symmetry direction Γ - K for (a) SL $\text{WS}_2/\text{Ag}(111)$ and (b) SL $\text{WS}_2/\text{Au}(111)$ (coverage ca. 0.7 ML in both cases, acquired at photon energy $h\nu=25$ eV; note that the Au bulk band structure is more strongly visible at this photon energy than the Ag band structure). The blue dashed lines are calculated bands for the highest VB and lowest conduction band of free-standing SL WS_2 , shifted such that the VB maximum coincides with the data measured here, and the conduction band minimum with the result of pump/probe time-resolved ARPES for SL $\text{WS}_2/\text{Ag}(111)$.³² We assume the same band gap for SL $\text{WS}_2/\text{Au}(111)$. (c) and (d) show magnifications of the regions in the coloured rectangles of (a) and (b), respectively, illustrating the additional intensity near the Fermi level for $\text{WS}_2/\text{Ag}(111)$, marked by a white arrow. (e)–(f) Photoemission intensity at the Fermi energy for $\text{WS}_2/\text{Ag}(111)$ and $\text{WS}_2/\text{Au}(111)$ ($h\nu=25$ eV). The enhanced diffuse photoemission intensity seen in (a) and (c) between Γ and K is visible in (e) and marked by white arrows. These states are almost absent for $\text{WS}_2/\text{Au}(111)$ and not found on clean $\text{Ag}(111)$.²¹

shift in the VB. While the shifted CB does indeed have a *local* minimum along Γ - K , at the so-called Q point, this state cannot give rise to the observed Fermi level crossing in a rigid band shift picture because the *absolute* CB minimum is found at K , not at Q , leaving the local minimum at Q well above the Fermi level.

Another possibility is that a distortion might occur in the lowest-lying CB, so as to pull the local minimum at Q down to the Fermi level while leaving the feature at K at a higher energy. Such band distortion could have several causes. Previous theoretical work has predicted this very effect as a result of in-plane compressive strain as small as 1%.⁴⁵ However, analysis of our LEED data rules out strain larger than $\pm 0.7\%$.²¹ Moreover, the lattice constant of Ag is larger than that of Au (4.09 Å for Ag versus 4.08 Å for Au), so it is unlikely that the WS₂ overlayer—if it is compressed—is more compressed on Ag than on Au.

The most likely explanation is that the distortion of the WS₂ CB that results in the metallicity of the layer is caused by hybridization with the underlying Ag states. Such hybridization with substrate states has recently been shown to be responsible for the aforementioned shift of the valence states at Γ toward higher binding energy than in the freestanding SL (see comparison between the calculated VB for a free standing layer and the actually observed dispersion in Fig. 2(a) and (b)).⁴⁴ Additionally, hybridization has been suggested as being responsible for important effects in other, related two-dimensional (2D) material systems; for example, as a source of “pseudo-doping” in metallic SL TaS₂ on Au(111).^{46,47}

We explore the possibility of hybridization in more detail using density functional theory calculations of SL WS₂ adsorbed on Ag(111) and Au(111). The resulting densities of states projected onto WS₂ (pDOS) for both substrates are shown in Fig. 3(a). The overall shift of the WS₂ states by 270 meV toward lower energies for WS₂/Ag(111) relative to WS₂/Au(111) agrees with the experimental binding energy shifts of Fig. 2. It is consistent with the lower work function of Ag, and the shift also leads to a smaller energy barrier between the metal Fermi level and the CB minimum of WS₂. Moreover, the calculated pDOS at the Fermi

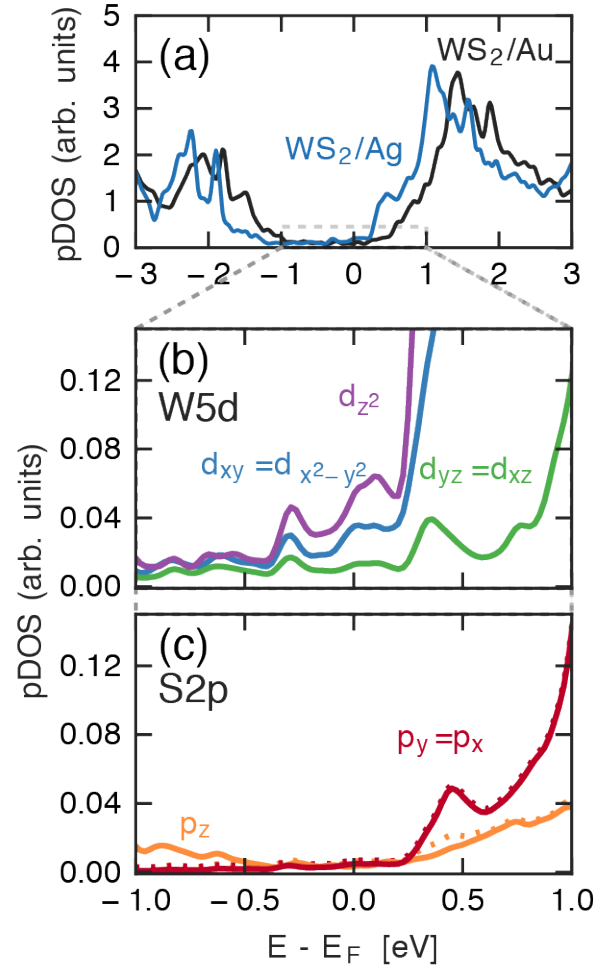


Figure 3: Origin of the metallic states in SL WS_2 on $Ag(111)$ from hybridization, viewed in terms of the density of states. (a) Calculated densities of states projected onto the WS_2 states of $Ag(111)$ and $Au(111)$ (pDOS). (b)–(c) Decomposed pDOS for W 5d and S 2p orbitals.

level of $\text{WS}_2/\text{Ag}(111)$ is indeed non-zero, due to the CB tailing into the band gap. This supports the observation of the metallicity of the WS_2 layer. We note that the conduction band actually tails into the band gap in both systems; it is the difference in relative distance between the Fermi level and the bottom of the CB that allows for a larger DOS at the Fermi level in the case of $\text{WS}_2/\text{Ag}(111)$.

We further elucidate the origin of the states at the Fermi level by decomposing the pDOS into contributions from the W 5d and the S 2p orbitals (Fig. 3(b),(c)). This reveals that the most significant contribution to the pDOS at the Fermi level stems from W d_{xy} , W $d_{x^2-y^2}$, and W d_{z^2} orbitals. These orbitals are also the ones giving the strongest contribution to the CB near Q for the free-standing WS_2 layer (see Figs. S3 and S4²¹ and ref.⁴⁸), suggesting that hybridization of the WS_2 CB with Ag states at this region of k -space is indeed responsible for the metallization of WS_2 .

This is confirmed by band structure calculations for the interacting system shown in Fig. 4. We start by plotting the band structure of free-standing WS_2 (red lines) together with that of a 20-layer surface model of bare $\text{Ag}(111)$ (gray lines) in Fig. 4(a) and do indeed find that regions of significant overlap between WS_2 and Ag bands (highlighted with black rectangles) correspond to k -vectors near Γ and Q for the VB and CB of SL WS_2 , respectively. To further clarify the effect of hybridization of the interacting bands, we have calculated the effective band structure of $\text{WS}_2/\text{Ag}(111)$ —*i.e.*, the effective weight of the bands in the large supercell when projected onto the 1×1 unit cell of the SL WS_2 . Fig. 4(b) shows the result of a calculation without SL substrate interaction for a bare 6-layer 4×4 $\text{Ag}(111)$ supercell together with the band structure of free-standing SL WS_2 , and Fig. 4(c) shows the effective band structure for the same system but including interactions. The smaller metal slab thickness used here leads to fewer bands crossing the Fermi level than for the 20-layer 1×1 unit cell shown in Fig. 4(a). Nevertheless, also here we identify crossings between WS_2 and Ag bands, which are indicated with black circles in Fig. 4(b). In the effective band structure in Fig. 4(c), these crossings are avoided due to band hybridization, which also results in Ag

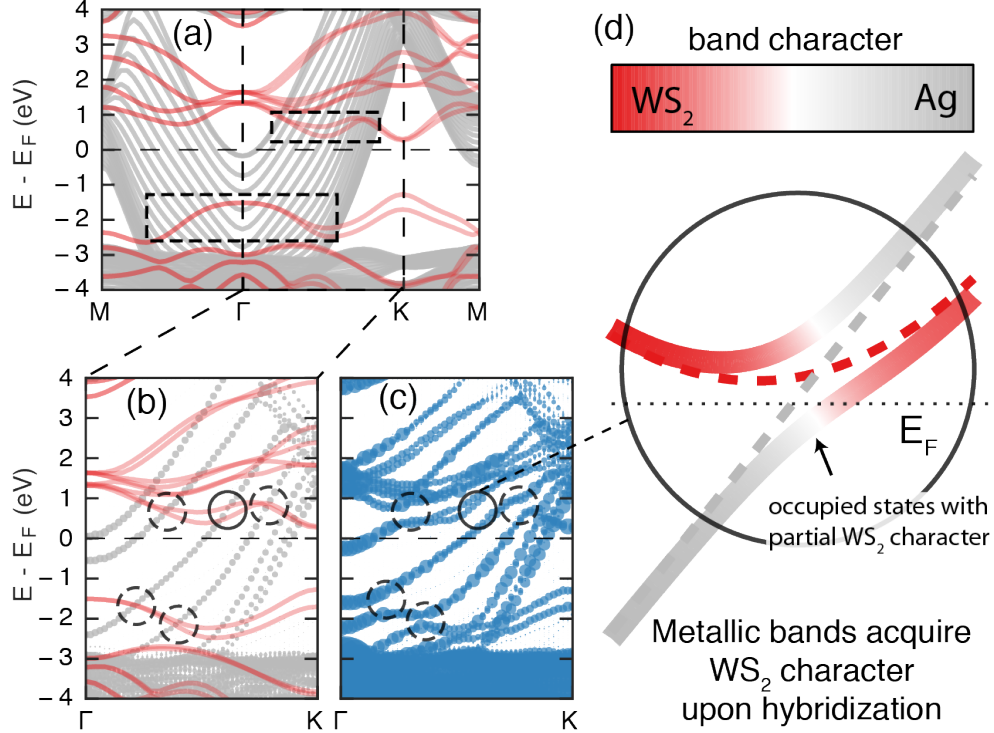


Figure 4: Origin of the metallic states in SL WS_2 on $\text{Ag}(111)$ from hybridization, viewed in a band structure picture. (a) Calculated band structure for free-standing SL WS_2 (red) together with the band structure of bare $\text{Ag}(111)$ (gray). Rectangles indicate the regions where Ag bands overlap with the valence and conduction bands of WS_2 . (b) Calculated band structure for free-standing SL WS_2 (red) together with the effective band structure of a 4×4 cell of $\text{Ag}(111)$. (c) Effective band structure of the supercell consisting of a $\sqrt{13} \times \sqrt{13}$ $R13.9^\circ$ of WS_2 on a 4×4 cell of $\text{Ag}(111)$. (d) Band hybridization leading to avoided crossing and partial character changes, as calculated from a simple two-state model. Thin dotted lines represent non-hybridized WS_2 and Ag bands. Thick solid lines represent the resulting hybridized bands and are colored according to their character as indicated in the overlying colormap. The solid circle in (b) and (c) corresponds to the situation depicted in (d).

and WS_2 bands acquiring partial WS_2 and Ag character, respectively.

For clarity, the effect of hybridization on the Ag and WS_2 bands is illustrated in Fig. 4(d), which shows the changes in band dispersion using a simple model with two interacting bands. The avoided crossing transforms one unoccupied band of WS_2 and one metallic band of Ag into two new bands (one unoccupied and one metallic) with varying Ag and WS_2 character. This effectively leads to an up-shift of the CBM of the unoccupied band, which is thus farther from the Fermi level and does not contribute to the metallicity of WS_2 . Instead, the formation of a hybridized metallic band gives rise to occupied states with partial WS_2 character, resulting in the metallic character of WS_2 . The occupied states of the metallic bands acquire the strongest contribution of WS_2 at k -vectors where the energy difference between the CB of WS_2 and the occupied Ag bands is smallest. This explains the dominant role of the CB near Q in the semiconductor-to-metal transition: the local CB minimum interacts with the Ag states, while the states at K , which constitute the absolute minimum in the CB of the noninteracting SL, do not. Since the CB of WS_2 is much closer to the Fermi level of Ag(111) than of Au(111), the hybridization mechanism can induce a semiconductor-to-metal transition only in the former case.

Conclusions

The results reported here show that metallization of a SL semiconductor can be achieved through substrate interaction. We emphasize that this effect depends on high interfacial quality, and would not be expected—at least in the material systems examined here—in samples prepared *ex situ* by means of, for example, “Scotch tape” style preparation. It would also not necessarily be expected to occur underneath polycrystalline metallic contacts evaporated thermally onto the top of SL devices, as in traditional device architectures. However, the fabrication is achieved by a straightforward, well-developed epitaxial approach that is easily adaptable for scalable production. Our results are achieved in WS_2 on Ag(111), but there

are presumably other material systems in which strong hybridization occurs between the electronic states of the SL and the substrate and in which similar (or even more dramatic) effects can be observed; identifying such systems remains a challenge for future work.

The finding that substrate interactions alone are sufficient to effect a transition from a semiconductor to a metal clears the path for major advances in 2D device fabrication. This result, in combination with earlier results showing the power of substrate interaction to tune band gap^{14,15} and doping,^{16,17} reduces the challenge of creating complex 2D device architectures from one of patterning the SL directly—a major challenge to date—to one of substrate choice and patterning, prior to covering the substrate with a homogenous SL semiconductor.

References

- (1) Tung, R. T. The physics and chemistry of the Schottky barrier height. *Applied Physics Reviews* **2014**, *1*, 011304.
- (2) Allain, A.; Kang, J.; Banerjee, K.; Kis, A. Electrical contacts to two-dimensional semiconductors. *Nature Materials* **2015**, *14*, 1195–1205.
- (3) Inkson, J. C. Many-body effect at metal-semiconductor junctions. II. The self energy and band structure distortion. *Journal of Physics C: Solid State Physics* **1973**, *6*, 1350.
- (4) Eda, G.; Fujita, T.; Yamaguchi, H.; Voiry, D.; Chen, M.; Chhowalla, M. Coherent Atomic and Electronic Heterostructures of Single-Layer MoS₂. *ACS Nano* **2012**, *6*, 7311–7317.
- (5) Kappera, R.; Voiry, D.; Yalcin, S. E.; Branch, B.; Gupta, G.; Mohite, A. D.; Chhowalla, M. Phase-engineered low-resistance contacts for ultrathin MoS₂ transistors. *Nature Materials* **2014**, *13*, 1128–1134.

- (6) Kappera, R.; Voiry, D.; Yalcin, S. E.; Jen, W.; Acerce, M.; Torrel, S.; Branch, B.; Lei, S.; Chen, W.; Najmaei, S.; Lou, J.; Ajayan, P. M.; Gupta, G.; Mohite, A. D.; Chhowalla, M. Metallic 1T phase source/drain electrodes for field effect transistors from chemical vapor deposited MoS₂. *APL Materials* **2014**, *2*, 092516.
- (7) Cho, S.; Kim, S.; Kim, J. H.; Zhao, J.; Seok, J.; Keum, D. H.; Baik, J.; Choe, D.-H.; Chang, K. J.; Suenaga, K.; Kim, S. W.; Lee, Y. H.; Yang, H. Phase patterning for ohmic homojunction contact in MoTe₂. *Science* **2015**, *349*, 625–628.
- (8) Song, S.; Keum, D. H.; Cho, S.; Perello, D.; Kim, Y.; Lee, Y. H. Room Temperature Semiconductor–Metal Transition of MoTe₂ Thin Films Engineered by Strain. *Nano Letters* **2016**, *16*, 188.
- (9) Kang, J.; Liu, W.; Sarkar, D.; Jena, D.; Banerjee, K. Computational Study of Metal Contacts to Monolayer Transition-Metal Dichalcogenide Semiconductors. *Physical Review X* **2014**, *4*, 031005.
- (10) Farmanbar, M.; Brocks, G. First-principles study of van der Waals interactions and lattice mismatch at MoS₂/metal interfaces. *Physical Review B* **2016**, *93*, 085304.
- (11) Wang, Y.; Yang, R. X.; Quhe, R.; Zhong, H.; Cong, L.; Ye, M.; Ni, Z.; Song, Z.; Yang, J.; Shi, J.; Li, J.; Lu, J. Does p-type ohmic contact exist in WSe₂-metal interfaces? *Nanoscale* **2016**, *8*, 1179–1191.
- (12) Gong, C.; Huang, C.; Miller, J.; Cheng, L.; Hao, Y.; Cobden, D.; Kim, J.; Ruoff, R. S.; Wallace, R. M.; Cho, K.; Xu, X.; Chabal, Y. J. Metal Contacts on Physical Vapor Deposited Monolayer MoS₂. *ACS Nano* **2013**, *7*, 11350–11357.
- (13) Ovchinnikov, D.; Allain, A.; Huang, Y.-S.; Dumcenco, D.; Kis, A. Electrical Transport Properties of Single-Layer WS₂. *ACS Nano* **2014**, *8*, 8174–8181.

- (14) Ugeda, M. M.; Bradley, A. J.; Shi, S.-F.; da Jornada, F. H.; Zhang, Y.; Qiu, D. Y.; Ruan, W.; Mo, S.-K.; Hussain, Z.; Shen, Z.-X.; Wang, F.; Louie, S. G.; Crommie, M. F. Giant bandgap renormalization and excitonic effects in a monolayer transition metal dichalcogenide semiconductor. *Nature Materials* **2014**, *13*, 1091.
- (15) Čabo, A. G.; Miwa, J. A.; Grønborg, S. S.; Riley, J. M.; Johannsen, J. C.; Cacho, C.; Alexander, O.; Chapman, R. T.; Springate, E.; Grioni, M.; Lauritsen, J. V.; King, P. D. C.; Hofmann, P.; Ulstrup, S. Observation of Ultrafast Free Carrier Dynamics in Single Layer MoS₂. *Nano Letters* **2015**, *15*, 5883–5887.
- (16) Rösner, M.; Steinke, C.; Lorke, M.; Gies, C.; Jahnke, F.; Wehling, T. O. Two-Dimensional Heterojunctions from Nonlocal Manipulations of the Interactions. *Nano Letters* **2016**, *16*, 2322–2327.
- (17) Komsa, H.-P.; Krasheninnikov, A. V. Effects of confinement and environment on the electronic structure and exciton binding energy of MoS₂ from first principles. *Physical Review B* **2012**, *86*, 241201.
- (18) Dendzik, M.; Michiardi, M.; Sanders, C.; Bianchi, M.; Miwa, J. A.; Grønborg, S. S.; Lauritsen, J. V.; Bruix, A.; Hammer, B.; Hofmann, P. Growth and electronic structure of epitaxial single-layer WS₂ on Au(111). *Physical Review B* **2015**, *92*, 245442.
- (19) Miwa, J. A.; Ulstrup, S.; Sørensen, S. G.; Dendzik, M.; Čabo, A. G.; Bianchi, M.; Lauritsen, J. V.; Hofmann, P. Electronic structure of epitaxial single-layer MoS₂. *Physical Review Letters* **2015**, *114*, 046802.
- (20) Grønborg, S. S.; Ulstrup, S.; Bianchi, M.; Dendzik, M.; Sanders, C. E.; Lauritsen, J. V.; Hofmann, P.; Miwa, J. A. Synthesis of Epitaxial Single-Layer MoS₂ on Au(111). *Langmuir* **2015**, *31*, 9700–9706.
- (21) See Supplemental Material for an estimate of the strain in the SL, for ARPES mea-

- measurements on clean Ag(111) and for the calculated orbital character of the SL WS₂ bands.
- (22) Hoffmann, S. V.; Søndergaard, C.; Schultz, C.; Li, Z.; Hofmann, P. An undulator-based spherical grating monochromator beamline for angle-resolved photoemission spectroscopy. *Nuclear Instruments and Methods in Physics Research, A* **2004**, *523*, 441.
 - (23) Kresse, G.; Hafner, J. Ab initio molecular dynamics for liquid metals. *Physical Review B* **1993**, *47*, 558–561.
 - (24) Kresse, G.; Furthmüller, J. Efficiency of ab-initio total energy calculations for metals and semiconductors using a plane-wave basis set. *Computational Materials Science* **1996**, *6*, 15–50.
 - (25) Kresse, G. Efficient iterative schemes for ab initio total-energy calculations using a plane-wave basis set. *Physical Review B* **1996**, *54*, 11169–11186.
 - (26) Blöchl, P. E. Projector augmented-wave method. *Physical Review B* **1994**, *50*, 17953–17979.
 - (27) Perdew, J.; Burke, K.; Ernzerhof, M. Generalized Gradient Approximation Made Simple. *Physical Review Letters* **1996**, *77*, 3865–3868.
 - (28) Popescu, V.; Zunger, A. Extracting E versus \vec{k} effective band structure from supercell calculations on alloys and impurities. *Physical Review B* **2012**, *85*, 085201.
 - (29) Medeiros, P. V. C.; Stafström, S.; Björk, J. Effects of extrinsic and intrinsic perturbations on the electronic structure of graphene: Retaining an effective primitive cell band structure by band unfolding. *Physical Review B* **2014**, *89*, 041407.
 - (30) Medeiros, P. V. C.; Tsirkin, S. S.; Stafström, S.; Björk, J. Unfolding spinor wave functions and expectation values of general operators: Introducing the unfolding-density operator. *Physical Review B* **2015**, *91*, 041116.

- (31) Steiner, S.; Khmelevskiy, S.; Marsmann, M.; Kresse, G. Calculation of the magnetic anisotropy with projected-augmented-wave methodology and the case study of disordered $\text{Fe}_{1-x}\text{Co}_x$ alloys. *Physical Review B* **2016**, *93*, 224425.
- (32) Ulstrup, S.; Čabo, A. G.; Biswas, D.; Riley, J. M.; Dendzik, M.; Sanders, C. E.; Bianchi, M.; Cacho, C.; Matselyukh, D.; Chapman, R. T.; Springate, E.; King, P. D. C.; Miwa, J. A.; Hofmann, P. Spin and Valley Control of Free Carriers in Single-Layer WS_2 . *Physical Review B* **2017**, *95*, 041405(R).
- (33) Füchtbauer, H. G.; Tuxen, A. K.; Moses, P. G.; Topsøe, H.; Besenbacher, F.; Lauritsen, J. V. Morphology and atomic-scale structure of single-layer WS_2 nanoclusters. *Physical Chemistry Chemical Physics* **2013**, *15*, 15971–15980.
- (34) Bruix, A.; Füchtbauer, H. G.; Tuxen, A. K.; Walton, A. S.; Andersen, M.; Porsgaard, S.; Besenbacher, F.; Hammer, B.; Lauritsen, J. V. *In Situ* Detection of Active Edge Sites in Single-Layer MoS_2 Catalysts. *ACS Nano* **2015**, *9*, 9322–9330.
- (35) Ulstrup, S.; Katoch, J.; Koch, R. J.; Schwarz, D.; Singh, S.; McCreary, K. M.; Yoo, H. K.; Xu, J.; Jonker, B. T.; Kawakami, R. K.; Bostwick, A.; Rotenberg, E.; Jozwiak, C. Spatially Resolved Electronic Properties of Single-Layer WS_2 on Transition Metal Oxides. *ACS Nano* **2016**, *10*, 10058–10067.
- (36) Doniach, S.; Šunjić, M. Many-electron singularity in X-ray photoemission and X-ray line spectra from metals. *Journal of Physics C: Solid State Physics* **1970**, *3*, 285–291.
- (37) Hüfner, S. *Photoelectron Spectroscopy*, 3rd ed.; Advanced Texts in Physics; Springer, 2003.
- (38) Citrin, P. H.; Wertheim, G. K.; Baer, Y. Many-body processes in x-ray photoemission line shapes from Li, Na, Mg, and Al metals. *Physical Review B* **1977**, *16*, 4256–4282.

- (39) Bruix, A.; Lauritsen, J. V.; Hammer, B. Effects of particle size and edge structure on the electronic structure, spectroscopic features, and chemical properties of Au(111)-supported MoS₂ nanoparticles. *Faraday Discussions* **2016**, *188*, 323–343.
- (40) Eda, G.; Yamaguchi, H.; Voiry, D.; Fujita, T.; Chen, M.; Chhowalla, M. Photoluminescence from Chemically Exfoliated MoS₂. *Nano Letters* **2011**, *11*, 5111–5116.
- (41) Acerce, M.; Voiry, D.; Chhowalla, M. Metallic 1T phase MoS₂ nanosheets as supercapacitor electrode materials. *Nature Nanotechnology* **2015**, *10*, 313–318.
- (42) Horcas, I.; Fernández, R.; Gómez-Rodríguez, J. M.; Colchero, J.; Gómez-Herrero, J.; Baro, A. M. WSXM: A software for scanning probe microscopy and a tool for nanotechnology. *Review of Scientific Instruments* **2007**, *78*, 013705.
- (43) Lizzit, S.; Pohl, K.; Baraldi, A.; Comelli, G.; Fritzsche, V.; Plummer, E. W.; Stumpf, R.; Hofmann, P. Physics of the Be(10 $\bar{1}$ 0) surface core level spectrum. *Physical Review Letters* **1998**, *81*, 3271–3274.
- (44) Bruix, A.; Miwa, J. A.; Hauptmann, N.; Wegner, D.; Ulstrup, S.; Grønberg, S. S.; Sanders, C. E.; Dendzik, M.; Grubišić Čabo, A.; Bianchi, M.; Lauritsen, J. V.; Khajetoorians, A. A.; Hammer, B.; Hofmann, P. Single-layer MoS₂ on Au(111): Band gap renormalization and substrate interaction. *Physical Review B* **2016**, *93*, 165422.
- (45) Amin, B.; Kaloni, T. P.; Schwingenschlögl, U. Strain engineering of WS₂, WSe₂, and WTe₂. *RSC Advances* **2014**, *4*, 34561–34565.
- (46) Sanders, C. E.; Dendzik, M.; Ngankeu, A. S.; Eich, A.; Bruix, A.; Bianchi, M.; Miwa, J. A.; Hammer, B.; Khajetoorians, A. A.; Hofmann, P. Crystalline and electronic structure of single-layer TaS₂. *Physical Review B* **2016**, *94*, 081404.
- (47) Wehling, T. O. Pseudodoping of Metallic Two-Dimensional Materials. *arXiv:1609.00220* **2016**.

- (48) Cappelluti, E.; Roldán, R.; Silva-Guillén, J. A.; Ordejón, P.; Guinea, F. Tight-binding model and direct-gap/indirect-gap transition in single-layer and multilayer MoS₂. *Physical Review B* **2013**, *88*, 075409.

ACKNOWLEDGMENTS

We gratefully acknowledge experimental help by Fabian Arnold and stimulating discussions with Silvano Lizzit. This work was supported by the Danish Council for Independent Research, Natural Sciences under the Sapere Aude program (Grants No. DFF-4002-00029 and No. 0602-02566B) and by VILLUM FONDEN via the Centre of Excellence for Dirac Materials (Grant No. 11744). A.B. acknowledges support from the European Research Council under the European Union's Seventh Framework Programme (FP 2007-2013)/Marie Curie Actions/Grant No. 626764 (Nano-DeSign).